

Rock failure assessment based on crack density and anisotropy index variations during triaxial loading tests

Kamran Panaghi^{1a}, Aliakbar Golshani^{*1} and Takato Takemura^{2b}

¹ Department of Civil and Environmental Engineering, Tarbiat Modares University, Jalal Ale Ahmad Highway P.O.Box: 14115-111, Tehran, Iran

² Department of Geosystem Sciences, College of Humanities and Sciences, Nihon University, 3-25-40 Sakurajyosui, Setagaya-ku, Tokyo 156-8850, Japan

(Received November 24, 2014, Revised June 11, 2015, Accepted October 30, 2015)

Abstract. Characterization of discontinuous media is an endeavor that poses great challenge to engineers in practice. Since the inherent defects in cracked domains can substantially influence material resistance and govern its behavior, a lot of work is dedicated to efficiently model such effects. In order to overcome difficulties of material instability problems, one needs to comprehensively represent the geometry of cracks along with their impact on the mechanical properties of the intact material. In the present study, stress-strain results from laboratory experiments on Inada granite was used to derive crack tensor as a tool for the evaluation of fractured domain stability. It was found that the formulations proposed earlier could satisfactorily be employed to attain crack tensor via the invariants of which judgment on cracks population and induced anisotropy is possible. The earlier criteria based on crack tensor analyses were reviewed and compared to the results of the current study. It is concluded that the geometrical parameters calculated using mechanical properties could confidently be used to judge the anisotropy as well as strength of the cracked domain.

Keywords: inada granite; crack tensor; triaxial test; fracture; tensor invariant

1. Introduction

Fabric characterization of cracked domains to assess engineering properties of discontinuous media are of special importance in the safety assessment of civil infrastructure such as road tunnels, nuclear waste repository sites, power plant and storage caverns. Geometrical changes during loading on rock specimens indicate that cracks will propagate differently depending on loading conditions. This suggests that preferential crack propagation can be induced considering orientation and magnitude of compression on specimens. In addition, the emergence of different crack types during the loading procedure refer to different micro-mechanisms in crack extensions. Up to the peak strength, the intra-granular cracks in rock minerals tend to propagate and damp fracture energy. The energy consumption in this manner is not high enough to trigger dynamic effects of emanated waves causing further crack propagation (Hazzard *et al.* 2000). As the peak

*Corresponding author, Assistant Professor, E-mail: golshani@modares.ac.ir

^a Ph.D. Candidate in Geomechanics, E-mail: k.panaghi@modares.ac.ir

^b Associate Professor, E-mail: takemura.takato@nihon-u.ac.jp

stress is achieved, the grain boundary cracks even the ones perpendicular to major loading direction form and the rock medium becomes disintegrated (Takemura and Oda 2004). It is believed that the sliding and rolling of the grains is responsible for the grain boundary cracks leading to failure. The blocky nature of specimens in this stage indicates that it no longer is a continuum with defects, but rather a discontinuous medium comprised of many sub-particles similar to soils.

Since the intertwined relationship between rock geometry and its mechanical properties is not negligible, many attempts by researchers have been focused on representing fractures in rock in a proper manner. The outcome, however, suffer inadequacy as they often require high-tech instruments. Monitoring acoustic emissions in which wave characteristics such as frequency are recorded and analyzed is a case in point. While some effort is done to model rock bursting failure, the varied distribution of cracks in different samples leads to inconsistent results (He *et al.* 2010). To overcome this deficiency, one needs to describe rock geometry so that it would be representative of the whole medium. Consequently, a Representative Elementary Volume (REV) should be assigned to test specimens which is also a function of the test type and the deemed degree of accuracy. Although the necessary specimen size for reliable results are different for different variables such as crack radii or crack density, Takemura and Oda (2004) showed that there is a threshold in which the propensity of experimental results to different causes of error is optimized to minimum. They concluded that a window size of at least six times the crack trace lengths is required to obtain statistically meaningful results for their experiments on Inada granite. Such uncertainty arises from the fact that the excavated surface in any construction site represents 2D distribution of cracks appearing in the form of crack traces and thorough understanding of the domain engineering properties via 3D studies is not possible. It is worth noting that micromechanical studies based on physically meaningful data are of high priority as they are easy to employ thanks to lower number of variables measurable by site surveying or laboratory experiments. Such micromechanical models for brittle failure have already been developed and implemented in the simulation of damaged zones in rocks (Golshani *et al.* 2006, 2007, Zhou *et al.* 2008, Golshani and Tran-Cong 2009, Zhou *et al.* 2010, Clayton 2010, Zhang *et al.* 2012).

In the present paper, the micromechanical characteristics of Inada granite are evaluated based on crack tensor analysis first introduced by Oda (1983). The analyses herein would be used to further discuss the phenomena related to macromechanical behavior of Inada granite under different confining pressures. Crack density changes and its effect on the rock behavior concerning the initiation of failure are scrutinized and conclusions based on the results of the current study and earlier research are drawn. This study serves as a complementary attempt in addition to those conducted earlier mainly by Oda and his colleagues. The current focus of this paper is to characterize crack density via mechanical investigations through triaxial tests on Inada granite. The present work is in line with the research conducted based on the stereological characterizations of fractured rock that facilitate discontinuous domain representations.

2. Crack tensor

2.1 Theory

Characterization of cracks in an otherwise continuous medium is of uttermost importance in the domain's mechanical behavior appraisals which are categorized into the following three forms:

- Volume Density (ρ): The number of cracks ($m^{(V)}$) represented by their centers in an REV defines the volume density of cracks: $\rho = m^{(V)}/REV$

The crack volume density in rock specimens is inversely proportional to the loading intensity; it decreases with an increase in axial loading. Takemura and Oda (2004) reported such trend in their experiments on Inada granite. The density was reported to be almost constant from 90 to 100 percent of maximum loads when stable crack growth occurred. Following failure of the specimens and further loading beyond the peak strength, a decrease in volume density was observed again which was attributed to unstable crack growth in the specimens. These results were in accordance with the observations made by Nemat Nasser and Horii (1983). The volume density of cracks is obviously a factor that inflicts rock strength. The higher number of cracks in a volume, the lower strength expected from rock specimens. Nonetheless, this factor alone lacks the coherent characteristics upon cracked domain assessments.

- Crack Dimension (r): The crack shape is idealized as flat and circular. This assumption is viable as Oda *et al.* (2002) produced bar graphs presenting crack trace lengths in three orthogonal planes all with almost similar distributions. As a result, the crack radius r can be obtained from the relationship $r = (S/\pi)^{1/2}$ in which S is the circular crack surface.

A probability density function such as $f(r)$ can then be defined to account for the distribution of cracks; describing the probability of occurrence of cracks with radii r to $r + dr$ via $f(r)dr$. It is recommended to identify $f(r)$ as

$$f(r) = \lambda \exp(-\lambda r) \quad (1)$$

since it is a simple equation with the mean and standard deviation both equal to $1/\lambda$. The function has to satisfy the following relationship

$$\int_0^{\infty} f(r) dr = 1 \quad (2)$$

More details can be found in Oda (1982).

- Crack Orientation (n): If the cracks are considered to be flat and circular, two unit normal vectors can be assigned to the corresponding two crack surfaces. Since only the sign of normal vectors are different, we introduce both as \mathbf{n} .

A probability density function $E(n)$ is then introduced to represent the crack orientations. Subsequently, $E(n)d\Omega$ would result in the probability of cracks whose unit normal vectors n would cover the solid angle $d\Omega$ (see Fig. 1).

The function $E(n)$ is symmetric in a manner that $E(n) = E(-n)$. This results from the opposite directions of unit normal vectors of two crack surfaces. The solid angle Ω stands for the surface of a unit sphere (4π) in which $0 \leq \alpha \leq 2\pi$ and $0 \leq \beta \leq \pi$. Similar to density function for crack sizes, $E(n)$ satisfies the following relationship

$$\iint_{\Omega} E(\mathbf{n}) d\Omega = 1 \quad (3)$$

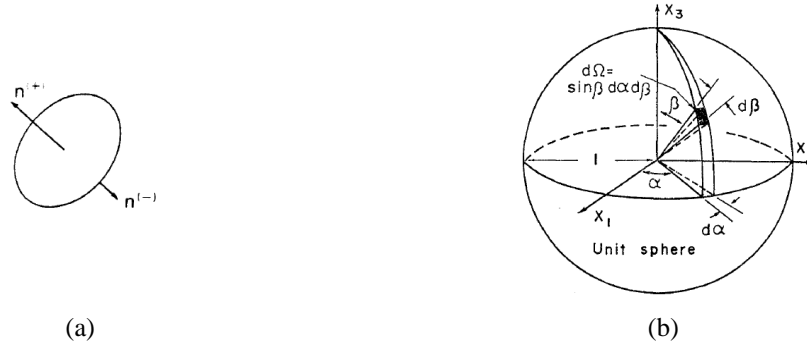


Fig. 1 (a) Unit normal vectors representing crack orientation (after Oda *et al.* 1986);
 (b) Unit sphere containing small solid angle $d\Omega$ (after Oda 1982)

Since coherent representation of cracks geometry requires all these factors to be taken into account, different researchers have proposed solutions to the problem (Kachanov 1980, Kawamoto *et al.* 1988). The results then obtained, though worth the effort, might lack the general practicality due to shortcomings related to the acquisition of data or the inclusion of all of the contributing factors. Oda *et al.* (1984) proposed a non-dimensional tensor \mathbf{F} that took all the density, size, and orientation of cracks into account. The crack tensor $F_{ij\dots k}$ in the integral form is written as

$$F_{ij\dots k} = \rho \int_0^\infty \int_0^\infty \int_\Omega 2Sr n_i n_j \dots n_k E(\mathbf{n}, r, S) d\Omega dr dS \quad (i, j, k = 1, 2, 3) \quad (4)$$

In the above formulation, $E(\mathbf{n}, r, S)$ is the probability density function of cracks that fall into the small solid angle $d\Omega$ with radii ranging from r to $r + dr$ and surface area from S to $S + dS$. The additive form of the above integral is

$$F_{ij\dots k} = \frac{1}{V} \sum_{p=1}^{m^{(v)}} 2S^{(p)} r^{(p)} n_i^{(p)} n_j^{(p)} \dots n_k^{(p)} \quad (i, j, k = 1, 2, 3) \quad (5)$$

In which V denotes the volume of the medium with defects. Since the crack tensor is symmetric, only tensors with even ranks would render non-zero components. The crack density F_0 can then be evaluated by calculating the first invariant of crack tensor \mathbf{F} . It is worthy of note that the crack density in this context embodies crack number density, crack size, and crack orientation as a whole and is a more comprehensive entity in comparison to the number of cracks in a representative volume. In light of field-measurable quantities used in crack tensor calculations, one can assume the practicality of the method. Furthermore, the analytical computations are easy to handle and no difficulty leading to alternate approach is arisen.

In a three dimensional space with principal axes of anisotropy F_1, F_2 , and F_3 , the second rank crack tensor can be depicted as vector \mathbf{OP} (see Fig. 2). Decomposing the vector into the space diagonal and its perpendicular component ($\mathbf{OP} = \mathbf{OA} + \mathbf{OB}$) leads to indicative measures by which the state of isotropy in the medium can be investigated. The deviatoric crack tensor is then calculated as

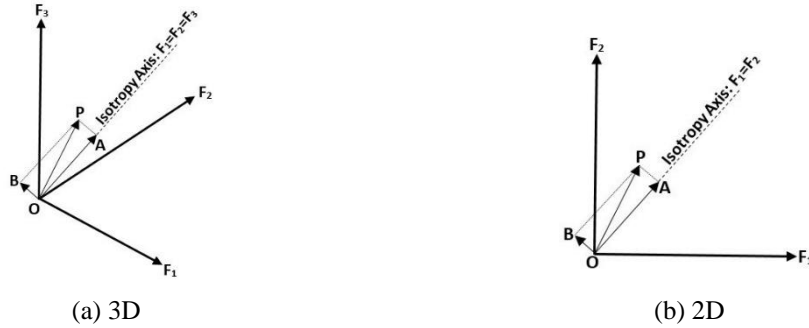


Fig. 2 Isotropic and anisotropic components of the crack tensor (reproduced after Oda, 1986)

$$F'_{ij} = F_{ij} - F_{kk}/3 \delta_{ij} \tag{6}$$

in which F'_{ij} is the deviatoric crack tensor and δ_{ij} is the Kronecker's delta. The ratio of the deviatoric vector length in the fabric anisotropy space to the corresponding isotropic component of crack tensor is a measure of anisotropy which for three dimensional analysis is represented as

$$A^{(F)} = \frac{|\mathbf{OB}|}{|\mathbf{OA}|} = \frac{\sqrt{6J_2}}{F_I} = \frac{[(F_1 - F_2)^2 + (F_2 - F_3)^2 + (F_3 - F_1)^2]^{1/2}}{F_1 + F_2 + F_3} \tag{7}$$

and as

$$A^{(F)} = \frac{|\mathbf{OB}|}{|\mathbf{OA}|} = \frac{F_1 - F_2}{F_1 + F_2} \tag{8}$$

for two dimensional studies.

2.2 Crack tensor determination

To attain crack tensor, one needs to employ a method that can capture crack property variations inside rock volume. Oda *et al.* (1984) rewrote Eq. (4) in petrographically measurable quantities as follows

$$F_{ij} = \frac{3\pi \langle l^2 \rangle}{8 \langle l \rangle} \frac{m^{(L)}}{h \langle |\mathbf{n} \cdot \mathbf{q}| \rangle} N_{ij} \tag{9}$$

In the above formulation

$$N_{ij} = \int_{\Omega} n_i n_j E(\mathbf{n}) d\Omega \tag{10}$$

and

$$\langle l^n \rangle = \int_0^{\infty} l^n \Phi(l) dl = \frac{1}{k} \sum_k l^n \tag{11}$$

where l is the trace length, $\Phi(l)$ is the trace probability density function, $m^{(L)}$ is the number of

cracks intersected by a scanning line with length h and direction of \mathbf{q} as the central axis of a cylindrical REV, and k is the number of crack lengths counted on the excavated surface.

$E(\mathbf{n})$ is a function of θ and ϕ if the orientation vector \mathbf{n} is described in the spherical coordinate system (see Fig. 3). Although similar to above, $E(\mathbf{n})$ can be obtained based on stereological based fabric analyses (e.g., Oda *et al.* 2002, Takemura *et al.* 2003), it can also be obtained via petrofabric methods (Douglas and Voight 1969). However, the latter tends to be laborious.

Oda *et al.* (1984) defined elastic compliance for cracked medium based on crack tensor in addition to Young's modulus and Poisson's ratio as elastic properties. The displacement jumps were determined for three types of penny shaped, elliptical, and row of collinear cracks and the average strains due to average stresses on the specimen were described in the following formula

$$\begin{bmatrix} \varepsilon_{11} \\ \varepsilon_{22} \\ \varepsilon_{33} \\ \varepsilon_{23} \\ \varepsilon_{31} \\ \varepsilon_{12} \end{bmatrix} = \frac{1}{D} \begin{bmatrix} F_{11} + \frac{D}{E} & -\frac{D}{E}\nu & -\frac{D}{E}\nu & 0 & \frac{1}{2}F_{13} & \frac{1}{2}F_{12} \\ & F_{22} + \frac{D}{E} & -\frac{D}{E}\nu & \frac{1}{2}F_{23} & 0 & \frac{1}{2}F_{12} \\ & & F_{33} + \frac{D}{E} & \frac{1}{2}F_{23} & \frac{1}{2}F_{31} & 0 \\ & & & \frac{F_{22} + F_{33}}{4} + \frac{D}{4G} & \frac{1}{4}F_{12} & \frac{1}{4}F_{31} \\ & Sym. & & & \frac{F_{33} + F_{11}}{4} + \frac{D}{4G} & \frac{1}{4}F_{23} \\ & & & & & \frac{F_{11} + F_{22}}{4} + \frac{D}{4G} \end{bmatrix} \begin{bmatrix} \sigma_{11} \\ \sigma_{22} \\ \sigma_{33} \\ 2\sigma_{23} \\ 2\sigma_{31} \\ 2\sigma_{12} \end{bmatrix} \quad (12)$$

in which G represents normal or shear stiffness as both were assumed to be equal in the elastic range where permanent crack surface displacements with respect to each other did not occur; and $1/D$ was regarded as $\pi/2E$ for elliptical cracks. The aforementioned is also prescribed in the present study since the derivation process requires no simplifying assumptions (Walsh 1965, Oda 1983). The corresponding relationship for two dimensional cases with elliptical cracks was further represented as

$$\begin{bmatrix} \varepsilon_{11} \\ \varepsilon_{22} \\ \varepsilon_{12} \end{bmatrix} = \frac{1}{E} \begin{bmatrix} \frac{\pi}{2}F_{11} + 1 & -\nu & \frac{\pi}{4}F_{12} \\ & \frac{\pi}{2}F_{22} + 1 & \frac{\pi}{4}F_{12} \\ Sym. & & \frac{\pi}{8}(F_{11} + F_{22}) + \frac{(1+\nu)}{2} \end{bmatrix} \begin{bmatrix} \sigma_{11} \\ \sigma_{22} \\ 2\sigma_{12} \end{bmatrix} \quad (13)$$

It is important to note that these formulations do not take microcracks interaction during loading

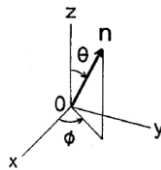


Fig. 3 Spherical coordinates in relation to the Cartesian coordinate system (after Kanatani 1985)

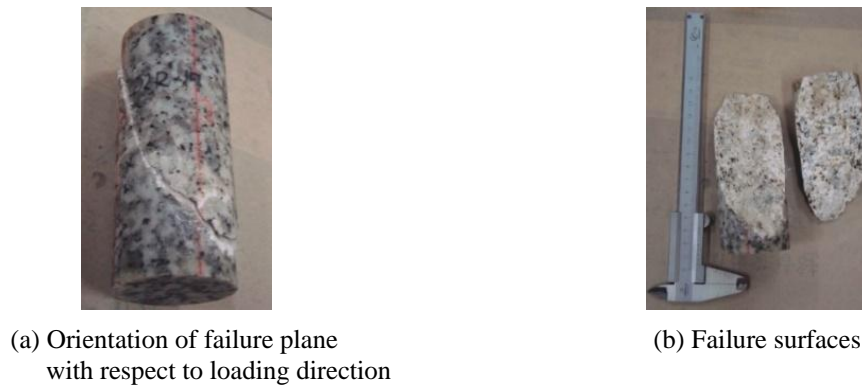


Fig. 4 Inada granite specimen after failure

into account which is crucial when the final stages of loading near specimen failure is achieved. Therefore, we either need to take an approach to assimilate cracks interaction in the behavioral law of the domain or implement a numerical scheme that automatically introduces such effects by nature. Oda *et al.* (1984) used the self-consistent method to study the developed formula above and concluded that the approach was capable of reproducing accurate enough results. However, the relation can also be used in numerical analyses that treat discontinuous domains as the conglomerate of smaller particles. In this case, the interaction among microcracks is accounted for by the equations based on which the code is built upon.

3. Procedure

3.1 Testing rock

Cylindrical samples of 12 cm in height and 5cm in diameter with average density of 2628 kg/m^3 were prepared by trimming top and bottom planes with a tolerance of 0.007 mm. The Inada granite samples were obtained from a quarry in Kasama, Ibaraki, Japan (Golshani 2003). Inada granite is composed of quartz (37%), alkali feldspar (24%), plagioclase (33%), biotite and other minerals (6%) (Suzuki *et al.* 1998). Takemura and Oda (2004) investigated crack density in Inada granite and attributed 70% of crack intensity to intra-quartz cracks. Intra-feldspar and grain-boundary cracks contributed to the number of defects to a lesser extent, respectively. Although the granite looks isotropic in appearance, three orthogonally oriented planes based on their compressive strength are distinguished namely in increasing order as hardway, grain, and rift. Fig. 4 depicts one Inada granite specimen after brittle failure due to axial loading perpendicular to rift plane. In the present study, experimental stress-strain results from triaxial tests on Inada granite under different confining pressures are used to obtain crack tensor indices of isotropy and anisotropy in lieu of stereological method. The results are then discussed and comparison with results derived from the stereological approach are drawn.

3.2 Calculation method

The current study implemented triaxial test results to calculate crack density changes with axial

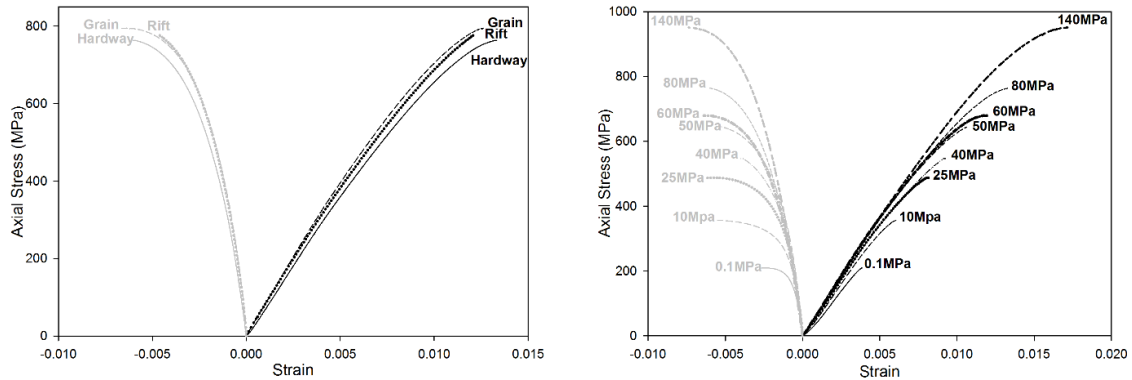
stress under different confining pressures obtained through the tests using the loading apparatus MTS Model 815 at Saitama University. This highly stiff loading system is capable of providing only one specific high pressure in the two main lateral directions. Initially, the hydrostatic pressure on the specimen was increased until it reached the pressure at which the confinement was aimed to be constant. Subsequently, the axial stress was increasingly applied until the occurrence of failure. The strain-controlled test was carried out such that the amount of circumferential strain in the loaded specimen accounted for the adjustment of the axial stress applied on it. Therefore, the circumferential strain rate was held at the constant rate of 5×10^{-6} mm/sec. Later on, the incremental changes of Poisson's ratio and Young's modulus were first calculated by employing the corresponding stress and strain values considering their axial and lateral measurements and the results were introduced into Eqs. (12) and (13) to obtain crack tensor diagonal terms for 3D and 2D formulations. Afterwards, crack tensor first invariants for each incremental change in the tensors were computed by the summation of crack tensor diagonal terms, and the anisotropy indices were derived based on Eqs. (7) and (8). The results were then prepared in graphical forms entailed with related discussions which contribute to the following sections.

4. Results and discussion

4.1 Poisson's ratio in rock

Although engineering materials most often take values between 0 and 0.5 for Poisson's ratio, it has been found that the value might considerably change for anisotropic media such as rock mass. The existence of cracks in rocks would lead to the decrease of Young's modulus; as it reduces the load bearing capacity of rocks. Unlike voids, cracks widths tend to diminish under compression causing the medium to attain elastic features once the load sustained is enough to close all cracks. However, the deformability of the domain is still different from the intact rock as crack surfaces might slip along each other. Walsh (1965) defined Poisson's ratio as the negative of the ratio of lateral strain rate to the axial ($\nu_{eff} = -d\varepsilon_{lateral} / d\varepsilon_{axial}$). This definition is helpful when materials with plastic or nonlinear behavioral characteristics are studied. Despite the common values of $0 \leq \nu \leq 0.5$ for most materials, it has been found that there are exceptions for a limited some in which the value is larger than 0.5 or even smaller than zero. One such instance in minerals is α Cristobalite for which $\nu = -0.164$ (Bass 1995). Such values suggest that the material extension would lead to lateral expansion of a rod-like specimen or vice versa for the material under compression and are explained by mineral twinning under load (Love 1944).

Fig. 5 illustrates the axial and lateral strains changes with the axial loading in different planes and confining pressures for Inada granite. The sign convention for the graphs below for compressive loading and the corresponding strains dictates positive magnitudes for axial strains (curves in black color) and negative values for the lateral strains (curves in grey). It can be observed that the effect of loading direction with regard to the three main planes of strength anisotropy in the rock are negligible (see Fig. 5(a)). As the confining pressure is increased, smaller axial and lateral strains are induced which result in closer placement of stress-axial strain and stress-lateral strain curves (see Fig. 5(b)). Based on the experimental data obtained via triaxial tests on Inada granite, the peak strengths associated with different confining pressures for the rock specimens were derived. Table 1 summarizes maximum axial strength of Inada granite specimens under various confinements. It is worthy of note that the values for Young's modulus and



(a) Loading under 80 MPa confining pressure for the three orthogonal planes (b) Loading perpendicular to Hardway plane under different confinements

Fig. 5 Axial stress-strain curves for Inada granite under triaxial loading conditions

Table 1 Maximum axial strength of Inada granite under different confining pressures

Confining Pressure (MPa)	0.1	10	25	40	50	60	80	140
Axial Strength (MPa)	209.1	355.8	488	546.8	635.1	679.6	763.5	951.1

Poisson’s ratio used in the current study were varying with the stress-strain changes in the specimen and therefore, no constant value for the aforementioned is reported. However, the values seemed to be close to the average values reported earlier by Golshani (2003).

Poisson’s ratio changes with increasing load increments were calculated from the data obtained via triaxial tests in which axial loading was applied in hardway plane direction (see Fig. 6). It is observed that the value of ν increases well beyond the acceptable 0.5 magnitude considered as an upper bound for engineering materials. Wittke (1990) indicated that transversely isotropic rocks may show larger than normal values for ν when loading direction is perpendicular to the bedding plane of rocks. Although the value of ν is stress independent for isotropic materials in general; Min and Jing (2004) reported that this value was stress dependent in jointed rock. Golshani (2003) carried out a series of experiments on Inada granite and derived E_{50} and ν_{50} as the engineering properties corresponding to that of intact rock. The values were determined by tangents to the axial stress-axial strain and lateral strain-axial strain graphs at 50% of peak strength. Since crack closure is assured under such condition, the values attained were considered as that of intact rock assuming linear elastic behavior. Taking average of the results, the values of $E = 73\text{GPa}$ and $\nu = 0.23$ were considered for the rock. It can be observed from Fig. 6 that the values of ν at the initial stages of loading are well lower than that of intact granite. This may be attributed to the open cracks that reduce material tendency to expand in the lateral direction. In the sequel stage, however, the value of ν begins to increase as the crack closure encourages linear elastic trend and the cracked rock behavior transforms into that of intact. In this stage, changes in the value of Poisson’s ratio reaches minimum as expected. Further loading causes the existing cracks to propagate during the stable crack growth phase and finally terminating in failure of the specimen due to coalescence of larger cracks (unstable crack growth). The results discussed herein are in accordance with similar studies found in literature (Bieniawski 1967, Krech *et al.* 1974). It is

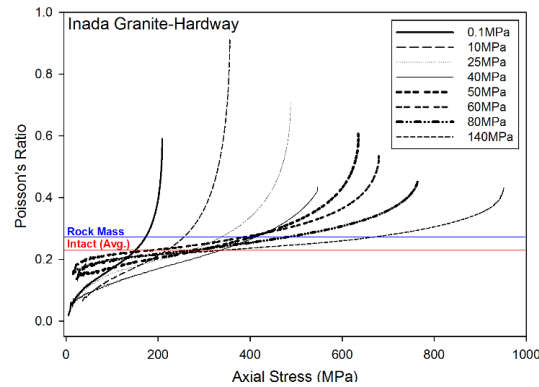


Fig. 6 Poisson's ratio changes of Inada granite with axial loading under various confining pressures

observed that the value $\nu = 0.23$ considered in earlier studies agrees with the elastic linear part of graphs by roughly meeting them in the half (red line). The scattered trend of the maximum calculated values of ν might be explained by the random nature of discontinuities in the rock domain where no certain distribution of cracks with various sizes and orientations is expected. In addition, steep changes in Poisson's ratio values become less pronounced by the increase in confining pressure and the range in which rock behaves elastically is broadened or in other words, more ductility is induced. As intuitively expected, higher confining pressures would result in higher axial strengths in cylindrical specimens. Kulatilake *et al.* (2004) proposed Poisson's ratio values for rock masses to be 20% higher than those of intact rocks due to the anisotropic behavior of the medium. It is also observed herein (blue line) that this value could serve as a crude estimate for the linear elastic trend's upper bound after which stable crack propagation initiates.

4.2 First invariant of crack tensor

As discussed, the first invariant of crack tensor F_0 represents crack density which can be used for the assessment of crack progress rate and the commencement of specimen failure. Oda *et al.* (2002) investigated F_0 variations with the anisotropy indices for Inada granite under confining pressures up to 140 MPa and concluded that a trend could be associated with specimens based on their failure mechanism. Consequently, two failure mechanisms were observed depending on the degree of specimen confinements. In the following, crack density variations with axial stress in three different orthogonal planes of Inada granite calculated by crack geometry dependent compliance tensors are compared with each other. The 2D stress-strain formulation based on crack geometry was first implemented for the calculations considering several confining pressures (see Figs. 7(a)-(c)). It should be noted that the data taken at the initial stages of loading might not be credible enough as it takes some adjustments regarding strain and stress gauges to be made before reliable measurements are obtained. Additionally, some data discrepancy in the final stages of loading might emerge from the normal trend observed during loading. One source of error in the measurements is the tripping of strain gauges producing anomalous data. In the current study, this error is subtly observed in the data measurements for the 40 MPa confinement of Inada granite in which limited number of less meaningful data are omitted near the specimen failure.

Fig. 7(d) compares the plots corresponding to three orthogonal planes under 40, 50, and 80 MPa confining pressures. It is obvious that the effect of confining pressure on F_0 values are more

pronounced than the loading planes and contradictory results for F_0 values taking plane stiffnesses into consideration might arise. Hence, for every set of data corresponding to one confining pressure a curve can be fitted by regression.

Oda *et al.* (1984) derived the following equation for the Young's modulus ratio of the cracked domain \bar{E} to that of the intact rock E

$$\frac{\bar{E}}{E} = \left(1 - \frac{\pi}{4} F_0\right) \tag{14}$$

Eq. (14) implies that the elasticity in discontinuous domain vanishes when the value of F_0 reaches 1.27. Under such condition, the cracks interconnect and form a network that act as pathways for fluid flow in permeability studies. Nonetheless, the cracked domain mechanical properties would still allow load bearing capacity since interlocking of discrete blocks and their rolling and slipping resistance would counteract instability. Later research (Oda *et al.* 2002) revealed that a value of $F_0 = 2.5$ for 2D models could be regarded as the upper bound for the crack density as a measure of severe damage. It is noteworthy that in the former study the self-consistent method (Budianski and O'Connell 1976) was used to treat interaction effect among

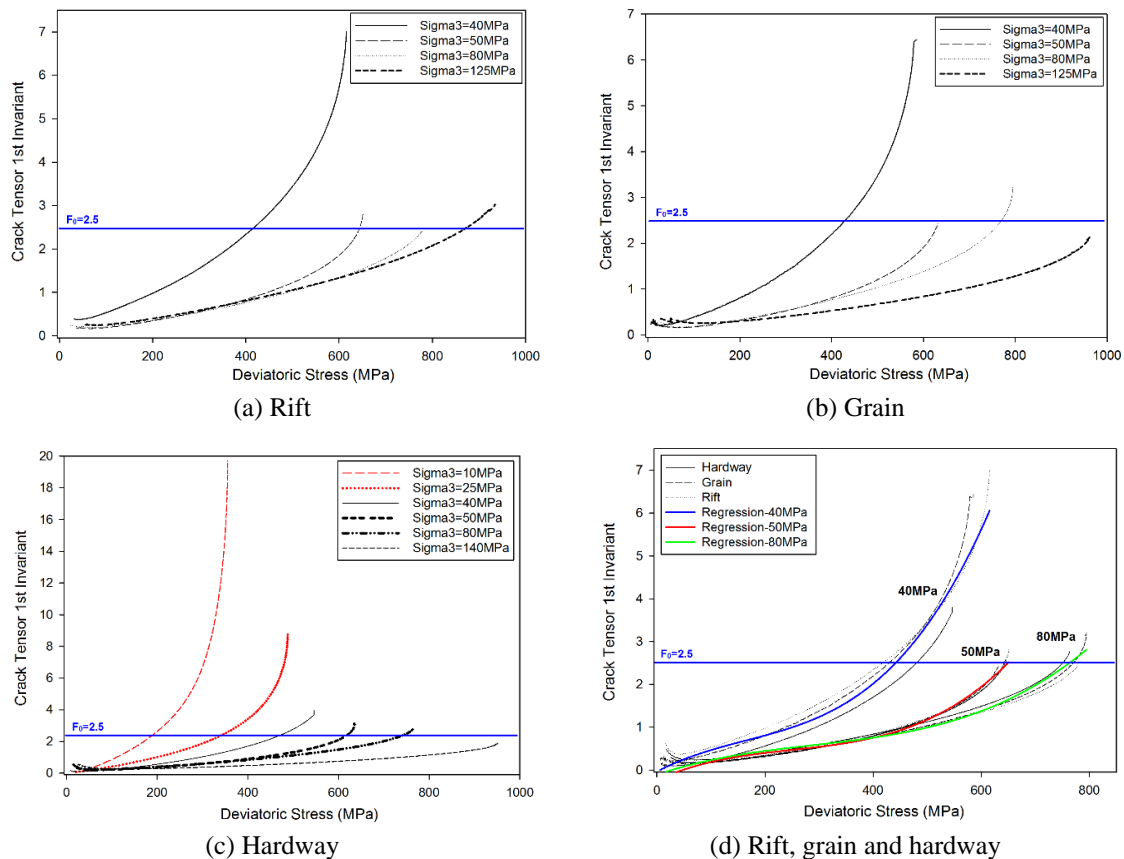


Fig. 7 2D crack density variations with axial stress under different confining pressures along the three orthogonal plane directions

cracks. It was shown that the results were affected by whether the interaction among cracks was taken into account and how it influenced rock behavior concerning crack density variations. It is seen that the first invariants of crack tensors calculated in the present study support the notion that this value can be a threshold for specimen failure. Some other observations are as follows:

- The F_0 values for specimens with confining pressures of 10 and 25 MPa (red lines in Fig. 7(c)) are well above the value suggested as the threshold for instability of cracked rock. It is noted, however, that the approach for calculating F_0 adopted herein is based on the micromechanics of cracked domains and any failure is described by cracks population. Contrary to that, there are cases where the failure mechanism under compression is assigned to critical stress intensity factor or material toughness at one or limited number of main crack tips that demand fracture mechanics concepts for further investigation. Laboratory results, for example, show that the uniaxial strength of specimens failed in compression is governed by the stress intensity factor at some crack tips. This behavior is also consistent for rock samples under low confining pressures up to 25 MPa as reported in Oda *et al.* (2002). As the confining pressure is increased, nonetheless, the failure mechanism tends to be better explained by the approach undertaken here.
- Since the crack tensor-dependent compliances adopted in the present study do not include interaction among cracks, the F_0 values for different confining pressures are presumably higher than those for more precise analyses taking interaction into account. Higher than the threshold F_0 values for the 40 MPa confining pressure on three different planes are in accordance with such speculation.
- The general trend of the plots in Figs. 7(a)-(c) indicates that the higher confining pressures are accompanied by lower values for crack density and subsequently higher compressive strengths for rock samples. Although the plot related to a 60 MPa confining pressure test results (not plotted) challenged the usual trend anticipated as compared to a 50 MPa confining pressure test in Fig. 7(c), they were still close enough; the probable reason for which is rock core anisotropy.
- The three orthogonal planes, i.e., rift, grain, and hardway characterize the compressive strengths of Inada granite core samples in the three orientations in descending order. Nevertheless, the measurements for overall elastic moduli of Inada granite in the three orthogonal directions show slight differences in magnitude (Golshani 2003). It can qualitatively be observed from Figs. 7(a)-(c) that the values of F_0 for the hardway plane are smaller than those of grain plane, those of which are smaller than the rift plane. These results support the fact that the density of induced cracks are less for planes of higher resistance to fracture.

The 2D calculations for F_0 threshold based on Eq. (13) accord well with the value proposed by Oda *et al.* (2002). They proposed that the value can serve as the threshold for structural disintegration of rock in which instability of tessellated rock blocks is induced after sliding resistance of interlocked domain is exceeded. Although a much smaller value is suggested for cracked domain permeability problems (Robinson 1984), the current value is high enough to account for the random distribution of cracks in a domain where block behavior is prevalent. Figs. 8(a)-(c) illustrate the results obtained from Eq. (12). Trends similar to 2D plots for 3D calculations of F_0 show that the earlier conclusions drawn for 2D studies can be generalized to 3D cases. However, it is observed that the threshold value for three dimensional cases is shifted to higher

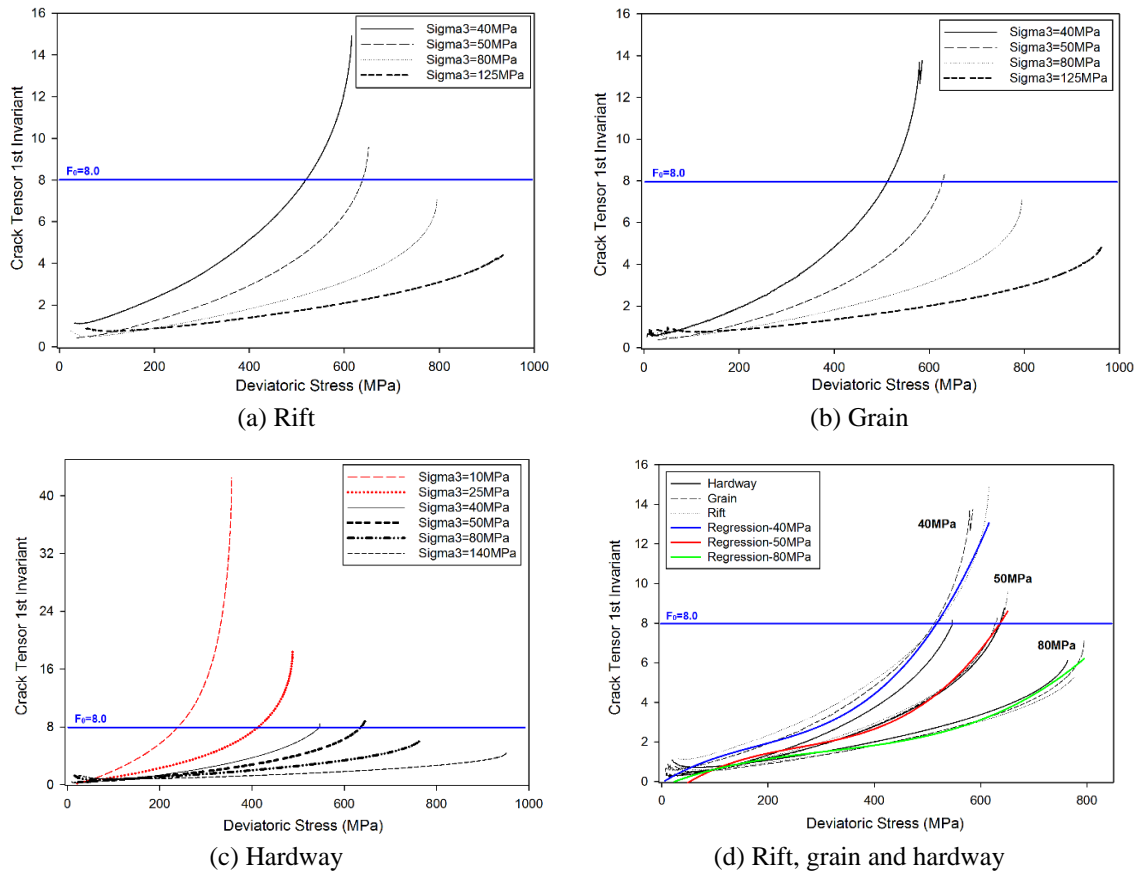


Fig. 8 3D crack density variations with axial stress under different confining pressures along the three orthogonal plane directions

values as compared to two dimensional studies. Oda *et al.* (2002) reported a value of 7 to 10 as the index for the instability of continuous domain with inherent defects. This value served as the limit beyond which rock domain was rather discrete with particular interaction. Later research by Takemura and Oda (2004) revealed that a value of 8.01 was more likely to represent disintegrated blocky domain of rock. They attributed such difference to the precision involved regarding the number of crack traces accounted for in the determination of crack tensors since traces smaller than a threshold length (1.0 mm in the former and 0.5 mm in the latter) were ignored. They also indicated an approximately linear trend for crack density increment with the inelastic volumetric strain which implies constant inelastic volumetric strains for specimens at peak failure. Fig. 8(d) illustrates 3D case results for the same confining pressures and planes depicted earlier in Fig. 7(d) for 2D cases. The same regression procedure is adopted for each set of curves and the remarks on 2D plots seem to be applicable for 3D cases as well.

4.3 Anisotropy in cracked medium

Oda (1982) reported that the length of vector **OB** in Fig. 2 can be related to rock anisotropy as

it represented deviatoric component of crack vector F . Since the length of OB is the numerator of the crack tensor anisotropy index, it is represented as

$$\Gamma = \sqrt{2J_2} = \sqrt{(F_1 - F_2)^2 + (F_2 - F_3)^2 + (F_3 - F_1)^2} \quad (15)$$

The calculated Γ above was not a comprehensive measure of anisotropy because it did not incorporate the deviation with respect to the space diagonal. Nevertheless, it can still be qualitatively said that some observations could be assumed to be viable if the relevant data are for a specific rock type and plane direction. Fig. 9 for example, represents the calculated values of Γ for Inada granite in hardway direction. The results are related to the confining pressures of 25, 40, 50, 80, and 140 MPa for specimens under a cycle of axial loading-unloading. The deviatoric vector length appears the largest for the smallest confining pressure and tends to be inversely proportional to the intensity of the aforementioned. Furthermore, the difference between two values of Γ for the same confining and axial pressures is reduced once an increase in lateral compression occurs. The dotted colored lines represent the limit of 70% of specimens' axial strength after which during loading and before which during unloading procedures AI attains constant values.

Since specimens are loaded beyond half their strength, the induced crack growth is most favorable (Paulding 1965) and hence the energy dissipation due to friction between cracks faces. The individual cycles of loading-unloading for specimens under different confinements would lead to a hysteresis-like loop in the Γ -axial stress plots whereas the changes in anisotropy index with axial stress beyond 70% of ultimate strength is approximately independent from loading (see Fig. 10(a)). This trend suggests that during the strain controlled test, the damage would continue to accumulate even when the core sample is unloaded. However, the ratio of Γ to the isotropic component of crack vector (F_0) becomes constant which is presumably due to higher rates of change for the isotropic component. Since the anisotropy index retains its value beyond and to 70% of material's ultimate strength during a loading-unloading cycle, this value marks the threshold for constant AI values. The threshold was determined based on the smaller than 0.0001 difference cutoff of two consecutive values for AI . It is interesting to note that the results for AI in the loading stage are almost identical with those of unloading. In addition, loading in three main plane orientations makes no difference concerning AI values (see Fig. 10(b)). The aforementioned are

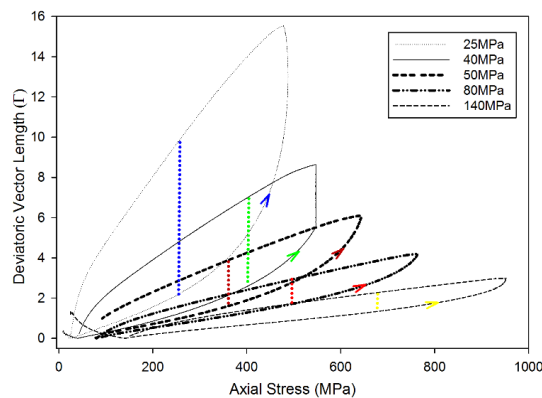


Fig. 9 Deviatoric vector length variations with axial stress in different confining pressures calculated from test results on specimens under one loading-unloading cycle-hardway plane (3D formulation)

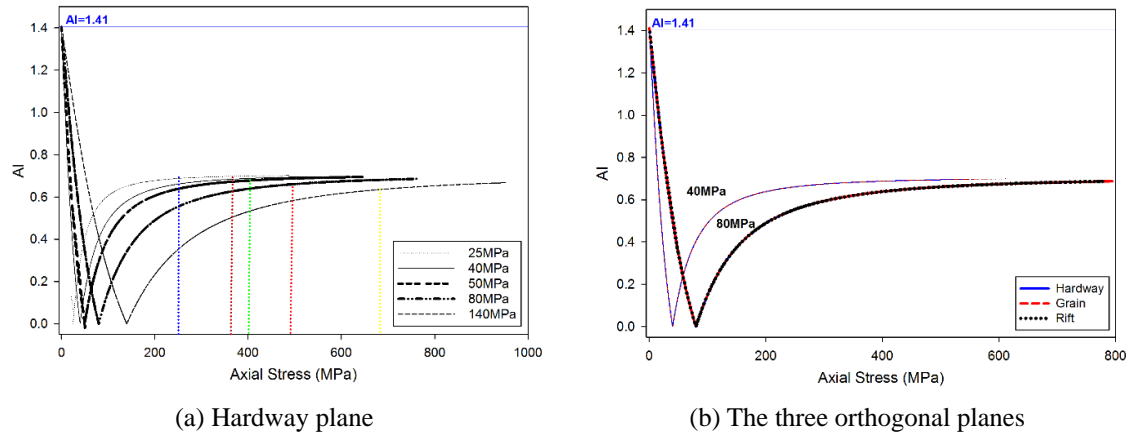


Fig. 10 Anisotropy index variations with axial stress in different confining pressures for Inada granite specimens under loading-unloading cycles (3D)

also valid for the set of plots related to 2D formulations (see Fig. 11). Walsh (1965) reported results for the stress-strain behavioral characteristics of Westerly granite considering axial, lateral, and volumetric strains. Unlike axial and lateral strain curves for loading-unloading cycles, the results formed no loops for the stress-volumetric strain changes. Therefore by analogy, one can associate axial and lateral strains with deviatoric vector as measures of failure assessment based on domain mechanical and geometrical properties, respectively. The same is applicable to volumetric strain and *AI* for one order higher.

Next, plots of *AI* changes with stress for 2D formulations are presented for the sake of comparison in Fig. 11. Again, the results seem to fall within the range proposed by Oda *et al.* (1986) and identical trends to previous results regarding crack density and anisotropy index appear to exist. The dotted colored lines pinpoint the same limit described earlier concerning Fig. (9). It should be noted that the values regarding 50 MPa confining pressure (not shown) were very close to those of 80 MPa so that the plots were difficult to detect from each other. However, as the

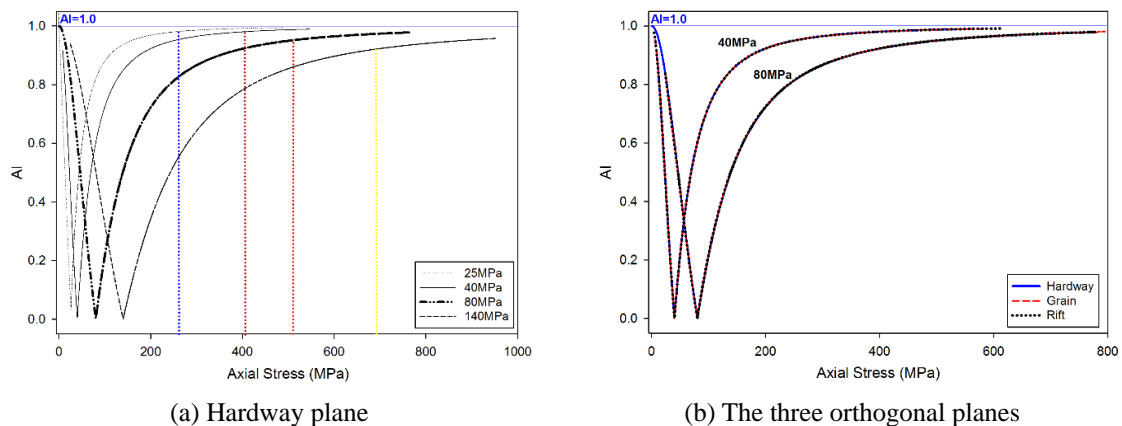


Fig. 11 Anisotropy index variations with axial stress in different confining pressures for Inada granite specimens under loading-unloading cycles (2D)

combination of anisotropy index with F_0 values are deterministic for cracked domains evaluations, such results will pose no drawback during investigations.

Another obvious trend in AI -stress plots is the steep decrease of AI to near zero values with axial stress in triaxial tests before axial stress equals the confining pressures (Figs. 12(a)-(b)). Since thickness of cracks in the formulation for crack tensor (Eq. (4)) is not taken into account,

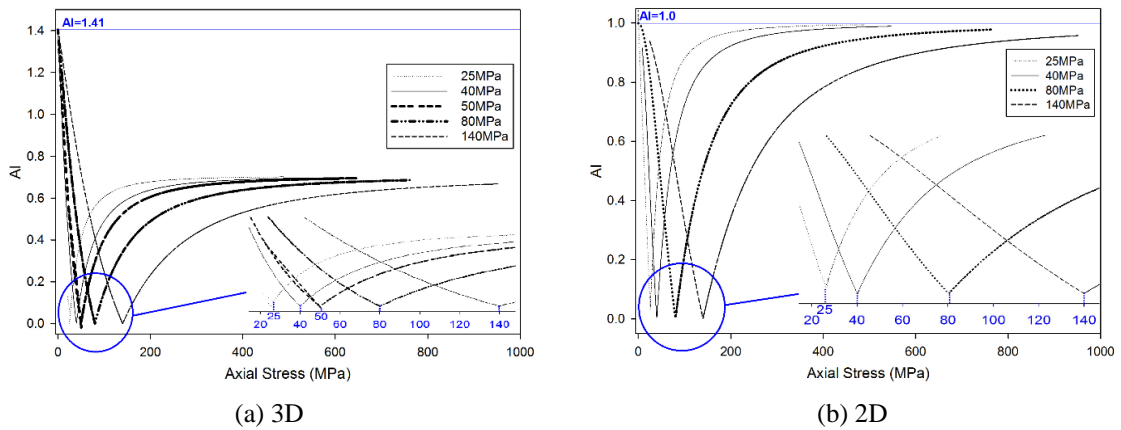


Fig. 12 Anisotropy index variations with axial stress in different confining pressures for Inada granite specimens under loading-unloading cycles

Table 2 Summary of calculated F_0 and AI values at specimens ultimate strength and threshold stresses for constant AI

Plane	Conf. Pre. (MPa)	Axial strength (MPa)	F_0 @Ult. Strength		AI @Ult. Strength		Threshold for Constant AI			
			2D	3D	2D	3D	2D	3D	2D	3D
Hardway	10	355.82	19.7	42	0.99	0.7	Stress (MPa)	Ratio*	Stress (MPa)	Ratio
	25	460.49	8.78	18.6	0.99	0.7	261.5	0.57	251.79	0.55
	40	546.78	3.95	8.47	0.99	0.7	405.82	0.74	401.73	0.73
	50	644.79	3.1	8.76	0.97	0.7	432.59	0.67	415.43	0.64
	80	736.52	2.76	6.12	0.98	0.69	510.16	0.69	492.18	0.69
	140	951.06	1.9	4.35	0.96	0.67	692.3	0.73	679.36	0.71
Grain	40	585.50	6.44	13.76	0.99	0.7	AI@Threshold Stress for Hardway Plane	Stress (MPa)	2D	3D
	50	632.23	2.43	8.32	0.97	0.7				
	80	794.85	3.23	7.11	0.98	0.69				
	125	962.62	2.15	4.85	-	-		25	0.9816	0.6883
Rift	40	615.76	7.0	14.92	0.99	0.7	40	0.9808	0.6882	
	50	650.99	2.8	9.57	0.97	0.7	50	0.9339	0.6720	
	80	777.83	2.4	7.11	0.98	0.69	80	0.9517	0.6600	
	125	934.71	3.02	4.42	-	-	140	0.9215	0.6350	

* Ratio of axial stress to specimen strength

Table 3 Summary of calculated F_0 and AI values for various loading intensities

Plane	Conf. Pre. (MPa)	LI* (%)	F_0										AI									
			2D					3D					2D		3D							
			50	60	70	80	90	50	60	70	80	90	50	60	70	80	90					
Hardway	10		2.14	2.96	4.03	5.67	8.64	4.66	6.40	8.67	12.16	18.49	0.993	0.995	0.996	0.997	0.997	0.700	0.702	0.703	0.704	0.705
	25		1.23	1.63	2.12	2.79	3.76	2.77	3.59	4.63	6.03	8.05	0.976	0.983	0.987	0.990	0.992	0.684	0.691	0.695	0.698	0.699
	40		0.89	1.19	1.57	2.03	2.66	2.03	2.67	3.46	4.43	5.75	0.958	0.970	0.978	0.983	0.986	0.668	0.679	0.686	0.691	0.694
	50		0.65	0.85	1.09	1.4	1.88	2.05	2.64	3.40	4.34	5.74	0.884	0.918	0.939	0.953	0.962	0.663	0.676	0.684	0.689	0.692
	80		0.75	0.95	1.17	1.45	1.79	1.83	2.25	2.72	3.29	4.02	0.909	0.936	0.952	0.963	0.971	0.628	0.650	0.663	0.673	0.679
	140		0.57	0.70	0.86	1.05	1.30	1.46	1.73	2.06	2.47	3.02	0.840	0.886	0.915	0.934	0.947	0.574	0.609	0.632	0.648	0.659
Grain	40		1.32	1.75	2.28	2.98	4.02	3.00	3.90	5.03	6.46	8.64	0.963	0.974	0.981	0.985	0.988	0.672	0.682	0.688	0.693	0.695
	50		0.56	0.74	0.95	1.23	1.63	2.00	2.60	3.33	4.26	5.59	0.880	0.914	0.936	0.951	0.961	0.662	0.675	0.683	0.688	0.692
	80		0.76	0.97	1.22	1.53	1.98	1.80	2.26	2.78	3.45	4.39	0.922	0.945	0.959	0.968	0.975	0.637	0.657	0.669	0.677	0.683
	125		0.64	0.80	0.98	1.20	1.50	1.60	1.92	2.30	2.78	3.43	-	-	-	-	-	-	-	-	-	-
	40		1.60	2.07	2.63	3.34	4.36	3.62	4.59	5.74	7.22	9.32	0.967	0.976	0.983	0.986	0.989	0.675	0.684	0.690	0.694	0.696
Rift	50		0.62	0.81	1.04	1.32	1.73	2.21	2.85	3.60	4.57	5.94	0.886	0.919	0.940	0.953	0.963	0.664	0.676	0.684	0.689	0.693
	80		0.74	0.93	1.16	1.43	1.78	1.76	2.19	2.70	3.32	4.17	0.919	0.943	0.957	0.967	0.974	0.635	0.655	0.667	0.676	0.682
	125		0.97	1.22	1.50	1.84	2.29	1.62	1.94	2.33	2.79	3.41	-	-	-	-	-	-	-	-	-	-
	40		1.60	2.07	2.63	3.34	4.36	3.62	4.59	5.74	7.22	9.32	0.967	0.976	0.983	0.986	0.989	0.675	0.684	0.690	0.694	0.696
	50		0.62	0.81	1.04	1.32	1.73	2.21	2.85	3.60	4.57	5.94	0.886	0.919	0.940	0.953	0.963	0.664	0.676	0.684	0.689	0.693

* Load Intensity (%)

both closed and open cracks can part in the discontinuous domain behavior. Consequently, as axial stress dictates cracks closure, more isotropy in the initial stages of loading is anticipated which is especially the dominant phenomenon before axial loading intensity reaches that of lateral pressure.

Table 2 summarizes some specific results for the current study. It is worth to point out that the ratios of the stress threshold for constant AI to ultimate strength for 2D and 3D formulations are both 0.7 corresponding to AI values of 0.95 and 0.7, respectively. However, more experiment on different types of rock is required before a conclusive remark on the values can be made. It is also observed that AI values do not exceed unity for 2D cases and 1.4 for 3D calculations. Takemura and Oda (2004) reported that cracks grew beyond grain boundaries when axial loading exceeded 90% of ultimate strength. The propagation of grain boundary cracks even the ones perpendicular to the loading direction accelerated near the failure of Inada granite samples, so that diagonal arrays of the tensor for the grain boundary cracks substantially increased. It was concluded that a new micromechanism different from the earlier crack initiation and growth pattern which results in the formation of shear bands might explain the notable inelastic volumetric strains. It should be noted that if the threshold for linear trend of AI -stress plots is altered toward more precision, closer magnitudes for the ratio in this study to the 90% value proposed by Takemura and Oda (2004) will be obtained (see Table 3).

Taking plots of 2D and 3D formulations of AI and F_0 into consideration, it is concluded that both sets refer to similar trends concerning crack anisotropy and density. It is reasonable to hold the 2D nature of loading accountable for such trend in the present study. It is also surmised that similar trends shall be obtained for uniaxial tests with zero confining pressure. On the contrary, distinguishable difference might arise for studies that employ true triaxial tests data that allow comparison between 2D and 3D cases.

5. Conclusions

In this study, we successfully used the experimental results on Inada granite along with stress-strain relationships based on crack tensor to appraise crack density and anisotropy of the discontinuous domain. The advantage of such approach lies behind the fact that easily measurable mechanical quantities extracted from laboratory experiments are enough to calculate the required criteria. Although the experimental limitations regarding shear loading would not allow us to obtain non-diagonal arrays of the crack tensor, the diagonal terms would only be needed for the crack concentration phenomena under investigation. However, further need for the calculation of non-diagonal terms would not impose difficulty as it can be achieved via stereological methods. Since the principal axes of fabric anisotropy are almost the same as the principal axes of crack tensor and the little rotation of axes happening especially in the final stages of loading is negligible, the calculation of non-diagonal arrays during and after loading procedure is reasonably circumvented by specifying the same arrays of the crack tensor for the starting specimens to the ones after experiments. Based upon the observations, the following conclusions are drawn:

- The F_0 values obtained for two and three dimensional studies are in accord with the general trend anticipated during axial loading. The threshold values obtained for a cracked medium under moderate to high confinements to manifest granular domain characteristics agree well with earlier studies implementing a different approach. The same applies for AI values as they decrease with higher confining pressures.
- The plots show that higher confining pressures result in higher axial strength for rock

specimens as they retard cracks initiation and propagation. Comparison between material strength in three different planes of Inada granite revealed that the effect of confining pressure on crack tensor's first invariant as a measure for damage is much more pronounced than its three main orientations of anisotropy. As the results suggest, the effect of plane anisotropy can be neglected by assigning a regression line to every set of plots representing different plane directions for one specific confining pressure. Results regarding AI changes with axial loading for different planes in Inada granite would further agree with this in a stronger manner.

- The results for AI values suggest a notable descending trend in the early stages of axial loading before it equals the lateral confinement which is due to cracks closure. This causes the cracked domain to behave more isotropically as the elastic behavior of rock matrix would dominate material behavior henceforth. Further loading would gradually induce inelastic behavior due to cracks growth which would ultimately lead to unstable growth of defects and constant AI for high axial stresses.
- It was found in an approximate manner that AI values for different confining pressures via 3D formulations attained a constant value of 0.7 after specimens were loaded to 70% of the final axial strength. In addition, values of AI for 2D formulations attained a constant value of approximately 0.95 with the same ratio of axial stress to ultimate strength. Although no conclusion can be made due to the results being restricted for one specific rock, further study as a tool for comparison might help explain such trends in other rock types, if available. Generally speaking, a different cracking phenomenon might be attributable to the failure mechanism of rock specimens after the stress threshold of 70% is surpassed. Since the details regarding crack types for crack tensor calculations were not considered in the current study, coherent judgment on the values is only feasible when different types of cracks are categorized and taken into account. Therefore, emphasis is laid upon the fact that our study was still restricted to elastic regime behavior in the rock matrix and further study that focus on the failure mechanism of samples in the final stages of loading is needed to render any conclusive remarks.

Acknowledgments

The authors would like to appreciate that some experimental data used in the current manuscript were obtained from Mr. T. Katsube's experimental work during his Master's degree study at Saitama University.

References

- Bass, J.D. (1995), "Elasticity of minerals, glasses and melts", In: *Mineral Physics and Crystallography: a Handbook of Physical Constants*, (T.J. Ahrens Ed.), American Geophysical Union, Washington D.C., USA.
- Bieniawski, Z.T. (1967), "Mechanism of brittle fracture of rock: parts 1 to 3", *Int. J. Rock. Mech. Min. Sci. Geomech. Abstr.*, **4**, 395-430.
- Budiansky, B. and O'Connell, R.J. (1976), "Elastic moduli of a cracked solid", *Int. J. Solids Struct.*, **12**(2), 81-97.
- Clayton, J.D. (2010), "Deformation, fracture, and fragmentation in brittle geologic solids", *Int. J. Fract.*, **163**(1), 151-172.

- Douglass, P.M. and Voight, B. (1969), "Anisotropy of granite: A reflection of microscopic fabric", *Geotechnique*, **19**(3), 376-398.
- Golshani, A. (2003), "A micromechanical model for brittle failure of rock under compression", Ph.D. Dissertation, Saitama University, Saitama, Japan.
- Golshani, A., Okui, Y., Oda, M. and Takemura, T. (2006), "A micromechanical model for brittle failure of rock and its relation to crack growth observed in triaxial compression tests of granite", *Mech. Mater.*, **38**(4), 287-303.
- Golshani, A., Oda, M., Okui, Y., Takemura, T. and Munkhtogoo, E. (2007), "Numerical simulation of the excavation damaged zone around an opening in brittle rock", *Int. J. Rock Mech. Min. Sci.*, **44**(6), 835-845.
- Golshani, A. and Tran-Cong, T. (2009), "Energy analysis of hydraulic fracturing", *KSCE J. Civil Eng.*, **13**(4), 219-224.
- Hazzard, J.F., Young, R.P. and Maxwell, S.C. (2000), "Micromechanical modeling of cracking and failure in brittle rocks", *J. Geophys. Res.*, **105**(B7), 16683-16697.
- He, M.C., Miao, J.L. and Feng, J.L. (2010), "Rock burst process of limestone and its acoustic emission characteristics under true-triaxial unloading conditions", *Int. J. Rock Mech. Min. Sci.*, **47**(2), 286-298.
- Kachanov, M. (1980), "Continuum model of medium with cracks", *Proc. of ASCE, Eng. Mech. Div.*, **106**(EM5), 1039.
- Kanatani, K. (1985), "Measurement of particle orientation distribution by a stereological method", *Part. Charact.*, **2**, 31-37.
- Kawamoto, T., Ichikawa, Y. and Kyoya, T. (1988), "Deformation and fracturing behavior of discontinuous rock mass and damage mechanics theory", *Int. J. Numer. Anal. Method. Geomech.*, **12**(1), 1-30.
- Krech, W.W., Henderson, F.A. and Hjelmstad, K.E. (1974), A standard rock suite for rapid excavation research; US Bur Min Rep Invest, 7865.
- Kulatilake, P.H.S.W., Park, J. and Um, J.G. (2004), "Estimation of rock mass strength and deformability in 3-D for a 30 m cube at a depth of 485 m at Äspö Hard Rock Laboratory", *Geotech. Geol. Eng.*, **22**(3), 313-330.
- Love, A.E.H. (1944), *A Treatise on the Mathematical Theory of Elasticity*, (7th Edition), Dover Publications, New York, NY, USA.
- Min, K.B. and Jing, L. (2004), "Stress dependent mechanical properties and bounds of Poisson's ratio for fractured rock masses investigated by a DFN-DEM technique", In: *Proceedings of Sinorock 2004 Symposium*, *Int. J. Rock Mech. Min. Sci.*, (J.A. Hudson and X.T. Feng Ed.), **41**(3), Paper 2A 13.
- Nemat-Nasser, S. and Horri, H. (1983), "Rock failure in compression", *Proceedings of the 9th Workshop Geothermal Reservoir Engineering*, Stanford University, Stanford, CA, USA, December.
- Oda, M. (1982), "Fabric tensor for discontinuous geological materials", *Soil Found.*, **22**(4), 96-108.
- Oda, M. (1983), "A new method for evaluating the effect of crack geometry on the mechanical behavior of cracked rock masses", *Mech. Mater.*, **2**(2), 163-171.
- Oda, M., Suzuki, K. and Maeshibu, T. (1984), "Elastic compliance for rock-like materials", *Soils Found.*, **24**(3), 27-40.
- Oda, M., Yamabe, T. and Kamemura, K. (1986), "A crack tensor and its relation to wave velocity anisotropy in jointed rock masses", *Int. J. Rock Mech. Min. Sci. Geomech. Abstr.*, **23**(6), 387-397.
- Oda, M., Katsube, T. and Takemura, T. (2002), "Microcrack evolution and brittle failure of Inada granite in triaxial compression tests at 140 MPa", *J. Geophys. Res.*, **107**(B10), 2233.
- Paulding, B.W. Jr. (1965), "Crack growth during brittle fracture in compression", Ph.D. Dissertation; Massachusetts Institute of Technology, Cambridge, MA, USA.
- Robinson, P.C. (1984), "Connectivity, flow and transport in network models of fractured media", Ph.D. Dissertation; Oxford University, Oxford, UK.
- Suzuki, K., Oda, M., Yamazaki, M. and Kuwahara, T. (1998), "Permeability changes in granite with crack growth during immersion in hot water", *Int. J. Rock Mech. Min. Sci.*, **35**(7), 907-921.
- Takemura, T. and Oda, M. (2004), "Stereology-based fabric analysis of microcracks in damaged granite", *Tectonophysics*, **387**(1-4), 131-150.
- Takemura, T., Golshani, A., Oda, M. and Suzuki, K. (2003), "Preferred orientations of open microcracks in

- granite and their relation with anisotropic elasticity”, *Int. J. Rock Mech. Min. Sci.*, **40**(4), 443-454.
- Walsh, J.B. (1965), “The effect of cracks on the uniaxial elastic compression of rock”, *J. Geophys. Res.*, **70**(2), 399-411.
- Wittke, W. (1990), *Rock Mechanics—Theory and Applications with Case Histories*, (R. Sykes Trans.), Springer, Berlin, Germany.
- Zhang, K., Zhou, H. and Shao, J. (2012), “An experimental investigation and an elastoplastic constitutive model for a porous rock”, *Rock Mech. Rock Eng.*, **46**(6), 1499-1511.
- Zhou, X.P., Zhang, Y.X., Ha, Q.L. and Zhu, K.S. (2008), “Micromechanical modelling of the complete stress–strain relationship for crack weakened rock subjected to compressive loading”, *Rock Mech. Rock Eng.*, **41**(5), 747-769.
- Zhou, J.W., Xu, W.Y. and Yang, X.G. (2010), “A microcrack damage model for brittle rocks under uniaxial compression”, *Mech. Res. Commun.*, **37**(4), 399-405.

CC